Commun. Comput. Phys.
doi: 10.4208/cicp.090110.270410a

Vol. **9**, No. 1, pp. 129-146
January 2011

Quantifying Tectonic and Geomorphic Interpretations of Thermochronometer Data with Inverse Problem Theory

G. Bao[1], Y. Dou[5], T. A. Ehlers[2], P. Li[3], Y. Wang[4] and Z. Xu[1,*]

[1] *Department of Mathematics, Michigan State University, East Lansing, MI 48824, USA.*
[2] *Institut fuer Geowissenschaften, Universitat Tuebingen, Germany.*
[3] *Department of Mathematics, Purdue University, West Lafayette, IN 47907, USA.*
[4] *Department of Mathematics, Fudan University, Shanghai, China.*
[5] *Department of Mathematics, Harbin Institute of Technology, Harbin, China.*

Received 9 January 2010; Accepted (in revised version) 27 April 2010

Available online 5 August 2010

Abstract. Thermochronometer data offer a powerful tool for quantifying a wide range of geologic processes, such as the deformation and erosion of mountain ranges, topographic evolution, and hydrocarbon maturation. With increasing interest to quantify a wider range of complicated geologic processes, more sophisticated techniques are needed. This paper is concerned with an inverse problem method for interpreting the thermochronometer data quantitatively. Two novel models are proposed to simulate the crustal thermal fields and paleo mountain topography as a function of tectonic and surface processes. One is a heat transport model that describes the change of temperature of rocks; while the other is surface process model which explains the change of mountain topography. New computational algorithms are presented for solving the inverse problem of the coupled system of these two models. The model successfully provides a new tool for reconstructing the kinematic and the topographic history of mountains.

AMS subject classifications: 86A22, 35R37, 35Q80, 86A60

Key words: Thermochronology, heat equations, inverse problem, variational method, iterative method, surface processes.

1 Introduction

In recent year, there has been growing interest in developing suitable numerical methods for studying geologic processes. A number of studies have been conducted demon-

*Corresponding author. *Email addresses:* bao@math.msu.edu (G. Bao), dou@math.msu.edu (Y. Dou), tehlers@me.com (T. A. Ehlers), lipeijun@purdue.edu (P. Li), zhengfu@math.msu.edu (Z. Xu)

strating how numerical modeling can improve the interpretation of geologic data, for example [3, 9, 13, 14, 17, 21]. Apatite (U-Th)/He thermochronometry has emerged as an important tool for quantifying the cooling history of rocks as they pass through the upper 1-3 km of the crust. The low closure temperature ($\sim$60°C) of this thermochronometer system has attracted interdisciplinary studies in the Earth science, such as for landform evolution, structural geology, geomorphology, geochemistry, petrology, and geodynamics [2, 7, 8, 22]. In general, thermochronometer data may be interpreted by measuring an age (or other related observables such as fission track lengths or noble gas release) from minerals extracted from rocks at or near the earth's surface. A thermonometer cooling age represents the time since a rock cooled below some effective closure temperature. These ages are influenced by either some events or geologic processes (e.g., erosion, faulting, topographic change, cooling of igneous rocks). In the latter case, which is closely related to our work in this paper, efforts are made to interpret the thermochronometer data to quantify the deformation, erosion, and topographic history of active mountain ranges. More specifically, we present in this paper a novel coupling of topographic evolution and 3D thermal models with inverse problem theory to reconstruct geologic processes. For thermal convection, the physical process is governed by

$$\rho c\left(\frac{\partial T}{\partial t}+\boldsymbol{v}\cdot\nabla T\right)=\nabla\cdot(k_1\nabla T)+\rho H. \tag{1.1}$$

Explanation of each of the terms and parameters will be given later. This equation is a classic heat equation defined on the three dimensional region with moving boundary, considering heat advection, diffusion and radiogenic effect. We also impose suitable boundary conditions based on the underlying physics and geologic setting. For surface process, we have another classic heat type equation, considering transportation by a surface velocity field, diffusivity of hillslope materials, and fluvial processes,

$$\frac{\partial S}{\partial t}=\nabla\cdot(k_2\nabla S)+\boldsymbol{u}\cdot\nabla S+u_3+a\sqrt{Q}\boldsymbol{d}\cdot\nabla S. \tag{1.2}$$

In this study, we do not include glacier erosion in the model because the governing equations are highly nonlinear problem and the evolution of mountain topography in many places can be described to a first order by Eq. (1.2). Our future work will focus on addressing glacial erosion. In Eq. (1.2), $\boldsymbol{v}=(v_x,v_y,v_z)$ is the velocity, $\boldsymbol{u}=(v_x,v_y)$ and $u_3=v_z$. For the inverse problem, the velocity $\boldsymbol{v}$ and surface $S(t,x,y)$ are the unknowns, which need to be reconstructed. The solution of the surface model serves as the moving boundary of the heat process. In our algorithm, we restore the velocity field by solving the inverse heat process model, and apply it as known to the surface model to obtain the initial surface by solving another inverse problem. This is carried out in an iterative fashion. To deal with the inverse problem entangled with a moving boundary, we freeze the boundary for a relatively short time period, by assuming that the mountain range does not change significantly in one thousand years.

A fundamental and yet often unquantified problem associated with thermochronometer data is that interpretations of geologic processes influencing their thermal history are not unique. The non-uniqueness of interpretations stems from two typical sources: multiple thermal histories (e.g., slow protracted vs. rapid cooling) can produce the same thermochronometer age [20]; trade-offs between different physical processes (e.g., heat flow into the base of the crust and erosion rate) can produce similar thermal histories thereby adding uncertainty to interpretations [11]. Fortunately, in many cases, these uncertainties can be reduced by appropriate sampling and analysis of multiple thermochronometer systems on the same sample. To quantify the geological process, we need to solve Eqs. (1.1) and (1.2) in a backward way. However the inverse problems of both the thermal convection and surface process are severely ill-posed, that is, small changes in the present temperature and surface may lead to a large deviation in the predicted velocity field and mountain surface in the past. The problem gets more serious in simulations of mountain evolution over millions of years. Several studies have investigated the numerical solution of the backward heat equations (1.1) and (1.2), for example [5,10]. Also, as well documented, the inverse problem to determine the coefficients of the lowest or leading terms for parabolic type equations is conditionally well-posed problem. Recent related results about the uniqueness and stability of recovery of certain coefficients of parabolic partial differential equations may be found in [4,6,15]. We refer to [19] and [23] for numerical reconstructions where the Tikhonov regularization is used and [16] for the quasi-solution method.

Our goal of this work is to numerically solve the inverse problem of the coupled system with the finite element method, assuming that one measurement of the temperature is available at every point and the current model topography is known. Our numerical results indicate that when the direction of the velocity field is known, (in practice, a priori guess of the direction of velocity field can be obtained from structural geology studies) the reconstruction of the velocity field can be accurate. However, the reconstruction of the initial surface is accurate when the simulation time is short and less so for a long time simulation due to its ill-posed nature. We also run the simulation for the coupled system, which incurs large computational cost.

The rest of the paper is outlined as follows. We introduce the formulation of the problems in Section 2 and the algorithm for solving inverse problem in Section 3. In Section 4, our initial numerical results for the coefficient inverse heat transport problem and the inverse surface process problem are presented. We also demonstrate the numerical results for the coupled system.

2 Formulation

We refer to [12] on modeling thermal dynamics in the Earth. It follows from the conservation of energy and Fourier's law for heat conduction that, at any point of the system $\boldsymbol{x}=(x,y,z)\in R^3$, the rate of change of temperature is proportional to the divergence of the

heat flux:

$$\rho c\frac{dT}{dt}=\nabla\cdot(k_1\nabla T),$$

where ρ is the density of the material, in this case the rocks, c is the capacity of the system, k_1 is the conductivity of the material and $T=T(t,\boldsymbol{x})$ is the temperature at $\boldsymbol{x}=(x,y,z)$ at time t.

If we consider that rocks are transported at a velocity $\boldsymbol{v}=(v_x,v_y,v_z)$ and there exists a temperature gradient in the material along that direction, we have

$$\begin{aligned}\frac{dT}{dt}&=\frac{\partial T}{\partial t}+\frac{\partial T}{\partial x}\frac{\partial x}{\partial t}+\frac{\partial T}{\partial y}\frac{\partial y}{\partial t}+\frac{\partial T}{\partial z}\frac{\partial z}{\partial t}\\&=\frac{\partial T}{\partial t}+\frac{\partial T}{\partial x}v_x+\frac{\partial T}{\partial y}v_y+\frac{\partial T}{\partial z}v_z\\&=\frac{\partial T}{\partial t}+\boldsymbol{v}\cdot\nabla T\end{aligned}$$

and

$$\rho c\Big(\frac{\partial T}{\partial t}+\boldsymbol{v}\cdot\nabla T\Big)=\nabla\cdot(k_1\nabla T). \tag{2.1}$$

On the earth, most rocks contain a finite concentration of radioactive isotopes, such as U, Th, and K. The decay of these radioactive atoms gives rise to an increased kinetic energy. By adding the contribution of the source to (2.1), we have

$$\rho c\Big(\frac{\partial T}{\partial t}+\boldsymbol{v}\cdot\nabla T\Big)=\nabla\cdot(k_1\nabla T)+\rho H,$$

where H is the rate of radiogenic heat production per unit mass. Let

$$D=\{(x,y)|0\le x\le a,0\le y\le b\},\qquad \Omega=\{(x,y,z)|(x,y)\in D,0\le z\le S\},$$

where $S=S(t,x,y)$ is the surface of the mountain at time t. We consider the heat transport process model, which satisfies the following equation with proper boundary conditions

$$\begin{cases}\rho c\left(\dfrac{\partial T}{\partial t}+\boldsymbol{v}\cdot\nabla T\right)=\nabla\cdot(k_1\nabla T)+\rho H,\\ T(t,x,y,S(t,x,y))=T_a, & (x,y)\in D,t_p\le t\le t_c,\\ T(t,x,y,0)=T_m, & (x,y)\in D,t_p\le t\le t_c,\\ \dfrac{\partial T}{\partial n}\Big|_{(x,y)\in\partial D}=0, & (x,y)\in\partial D,t_p\le t\le t_c,\\ T(t_p,x,y,z)=T_p(x,y,z), & (x,y,z)\in\Omega,t_p\le t\le t_c.\end{cases} \tag{2.2}$$

Here density of material ρ, capacity c, conductivity k_1, rate of radiogenic heat production per unit mass H could be obtained by experiments. The boundary value T_a is the temperature of air and T_m is the temperature at the base of the crust or asthenosphere. These

two parameters are reasonably well known and initial temperature distribution $T_p(x,y,z)$ is also well constrained. The vertical side boundaries are assumed to be conductively isolated, $\partial T/\partial n=0$. For the inverse problem, the velocity v and surface $S(t,x,y)$ are unknown, which need be reconstructed. The measurement data is $T(t,\boldsymbol{x}_j(t))$, $j=1,\cdots,m$, the history temperature data at points $\boldsymbol{x}_j(t)$. But actually even we know $\boldsymbol{x}_j(t_c)$, the current location of measurement points, but do not know the history location of the measurement points $\boldsymbol{x}_j(t)$, $t_p\leq t<t_c$. To overcome this difficulty, it is assumed that the location is only changed by the velocity at this point

$$\boldsymbol{x}_j(t)=\boldsymbol{x}_j(t_c)-\int_t^{t_c}\boldsymbol{v}dt.$$

Another model is the surface process model, where three mechanisms are involved: the hillslope process, the advection and uplift, and the fluvial process.

First, diffusion is used to represent a variety of surficial hillslope processes over long time scales, including regolith creep and mass wasting by bedrock-involved landslides, which describes the time dependent change on the surface of the earth,

$$\frac{\partial S}{\partial t}=\nabla\cdot(k_2\nabla S). \tag{2.3}$$

Here $S=S(t,\mathbf{x})$, $\mathbf{x}=(x_1,x_2)\in R^2$ is the height function of $\mathbf{x}$ at time t, and k_2 is the diffusivity constant. If combined with an uplift by the velocity u_3 and a horizontal transport by the velocity $\boldsymbol{u}=(u_1,u_2)$, the equation (2.3) describing the change of surface can be changed to

$$\frac{\partial S}{\partial t}=\nabla\cdot(k_2\nabla S)+\boldsymbol{u}\cdot\nabla S+u_3.$$

Now we take the fluvial process into consideration. Define Q as the discharge L^3/t, ℓ as the direction of the river. Sediment is not considered in this model because bedrock channels in mountainous settings often have a sediment load less than the capacity and thus it is reasonable to believe there is no sediment storage. The bedrock incision at a rate of $\frac{\partial S}{\partial t}$, also taken to be proportional to stream power

$$\frac{\partial S}{\partial t}=\frac{k_f}{w}Q\frac{\partial S}{\partial \ell},$$

where w is the channel width and k_f is a proportionality constant. The channel width is assumed to be proportional to the square root of discharge

$$w=a\sqrt{Q}.$$

Finally

$$\frac{\partial S}{\partial t}=\nabla\cdot(k_2\nabla S)+\cdot\nabla S+u_3+\frac{k_f}{a}\sqrt{Q}\frac{\partial S}{\partial \ell}.$$

By combining all of the factors considered above, we have the following equations for the surface process model

$$\begin{cases} \dfrac{\partial S}{\partial t} = \nabla\cdot(k_2\nabla S)+\boldsymbol{u}\cdot\nabla S+u_3+a\sqrt{Q}\boldsymbol{d}\cdot\nabla S, \\ \dfrac{\partial S}{\partial n}\Big|_{\partial D}=0, \\ S(t_p,x,y)=S_p(x,y), \qquad (x,y)\in D, t_p\le t\le t_c. \end{cases} \tag{2.4}$$

Here the diffusivity constant of hillslope processes is given by k_2, proportional constant a, river channel discharge Q and direction $\boldsymbol{d}$ are known from historic data or by experiments. The functions $\boldsymbol{u}$ and u_3 are the velocity $\boldsymbol{v}$ on the surface. Our objective is to reconstruct $S_p(x,y)$ from $S_c(x,y)$.

The model problem is a coupled system because $\boldsymbol{u}$ and u_3 of the surface process model come from the velocity $\boldsymbol{v}$ of the heat transport process model, while the top boundary of the domain for the heat transport process model comes from the solution of surface process model. In the following, we abbreviate the heat transport process model and the surface process model by HTPM and SPM, respectively.

3 Algorithm

For simplicity, we assume that the velocity $\boldsymbol{v}$ is a piecewise constant function with respect to t

$$\boldsymbol{v}(t,x,y,z)=\boldsymbol{v}(t_i,x,y,z), \quad t_i\le t<t_{i+1},$$

where $t_p=t_0<t_1<\cdots<t_N=t_c$ is a partition of $[t_p,t_c]$.

We also assume that

$$S(t,x,y,z)=S(t_i,x,y,z), \quad t_i\le t<t_{i+1},$$

such that we can solve the forward problem of the heat transport process model in a fixed domain when $t_i\le t<t_{i+1}$.

The iteration is as follows:

First, we give the initial guess of the velocity $\mathbf{v}^{(k)}(t_i,x,y,z)$, $i=0,1,\cdots,N-1$ and the initial guess of the surface at time t_p: $S_p^{(k)}(x,y),(x,y)\in D$, where $S_p^{(k)}(x,y)$ is also the surface between time $[t_0,t_1]$, also denoted as $S_0^{(k)}(x,y),(x,y)\in D$. Here k is the count of the iterations, where $k=0$ at the beginning.
Next, we update $\mathbf{v}$ from $T(t,\mathbf{x}_j(t))$, $j=1,\cdots,m$, assuming that $S_0(x,y)$ is fixed.
Then update $S(t_p,x,y)$ from the current surface $S(t_c,x,y)$, assuming that $\mathbf{v}$ is known.

Repeat the previous steps until certain stopping criterion is met.

Next the details for updating the velocity field and surface are discussed. To update S and V, we adopt the gradient method by minimizing the cost functional in the L_2 norm. To obtain the gradient of the cost functional, two backward heat type equations are solved.

3.1 Update v when $S_0(x,y)$ is fixed

Step 1: With the current $\mathbf{v}^{(k)}(t_i,x,y,z)$, $i=0,1,\cdots,N-1$, we can obtain $\mathbf{u}(t_i,x,y)$ and $u_3(t_i,x,y)$ for $i=0,1,\cdots,N-1$. With the guess of initial surface $S_0^{(k)}(x,y)$, we solve the surface process model as a forward problem for

$$S_i(x,y)=S(t_i,x,y),\quad (x,y)\in D,\quad i=0,1,\cdots,N.$$

Step 2: Solve the heat transport process model for $t_0\le t\le t_1$ with the velocity $\mathbf{v}^{(k)}(t_0,x,y,z)$. The initial temperature $T_0=T_p$ is given. The temperature at t_1 is denoted as T_1 which is used as the initial value of the forward problem for $t_1\le t\le t_2$.

Step 3: Update $\mathbf{v}^{(k)}(t_0,x,y,z)$ from the measurement data $T(t,\mathbf{x}_j(t))$,$t_0\le t\le t_1$. The detailed algorithm for updating $\mathbf{v}^{(k)}(t_0,x,y,z)$ is provided below.

Step 4: Repeat Step 2 and Step 3 for $t_i\le t\le t_{i+1}$, $i=1,2,\cdots,N-1$.

Thus, we finish one cycle of iteration for updating v.

To update $\boldsymbol{v}^{(k)}(t_i,x,y,z)$, we adopt a variational approach for the heat transport process model for $t_i\le t\le t_{i+1}$. Let $\tilde{\boldsymbol{v}}=\boldsymbol{v}+\delta\boldsymbol{v}$, T be the solution of the heat transport process model with the velocity $\boldsymbol{v}$ and $\tilde{T}$ be the solution with the velocity $\tilde{\boldsymbol{v}}$. Let $\delta T=\tilde{T}-T$. It is clear that the initial values are the same: $\tilde{T}_i=T_i$. Hence δT satisfies the following equations

$$\begin{cases} \rho c\left(\dfrac{\partial(\delta T)}{\partial t}+\boldsymbol{v}\cdot\nabla(\delta T)\right)=\nabla\cdot(k_1\nabla(\delta T))-\delta\boldsymbol{v}\cdot\nabla T, & \\ \delta T(t,x,y,S(t,x,y))=0, & (x,y)\in D, \\ \delta T(t,x,y,0)=0, & (x,y)\in D, \\ \dfrac{\partial(\delta T)}{\partial n}\Big|_{(x,y)\in\partial D}=0, & (x,y)\in\partial D, \\ \delta T(t_i,x,y,z)=0, & (x,y,z)\in\Omega, \end{cases} \tag{3.1}$$

where $\Omega=D\times S_i(x,y)$. Define the cost functional

$$J(\boldsymbol{v})=\frac{1}{2}\sum_{j=1}^{m}\int_{t_i}^{t_{i+1}}(T(t,\boldsymbol{x}_j)-Z(t,\boldsymbol{x}_j))^2+\alpha\int_\Omega|\boldsymbol{v}|^2=J_1+J_2. \tag{3.2}$$

Since it is assumed that there is no movement in time $[t_i,t_{i+1}]$, $\boldsymbol{x}_j$ now is independent of time t for every j. To minimize the cost functional (3.2) by a gradient method, let

$$\zeta_j(t)=\zeta(t,\boldsymbol{x}_j)=T(t,\boldsymbol{x}_j)-Z(t,\boldsymbol{x}_j).$$

Thus

$$J_1(\tilde{\boldsymbol{v}})-J_1(\boldsymbol{v})=\frac{1}{2}\sum_{j=1}^{m}\int_{t_i}^{t_{i+1}}\delta T(t,\boldsymbol{x}_j)(\tilde{T}(t,\boldsymbol{x}_j)+T(t,\boldsymbol{x}_j)-2Z(t,\boldsymbol{x}_j)).$$

Therefore

$$J_1'(\boldsymbol{v})\delta\boldsymbol{v}=\int_{t_i}^{t_{i+1}}\sum_{j=1}^{m}T'(t,\boldsymbol{x}_j)\delta\boldsymbol{v}\zeta_j(t) \tag{3.3}$$

or

$$J_1'(\boldsymbol{v})=\sum_{j=1}^{m}T'(t,\boldsymbol{x}_j)\zeta_j(t),$$

where T' is the Fréchet derivative with respect to $\boldsymbol{v}$. Consider the adjoint problem

$$\begin{cases}\rho c\left(\dfrac{\partial W}{\partial t}+\nabla\cdot(\boldsymbol{v}W)\right)=-\nabla\cdot(k_1\nabla W)-\displaystyle\sum_{j=1}^{m}\zeta_j(t)\delta(\boldsymbol{x}-\boldsymbol{x}_j),\\ W(t,x,y,S(t,x,y))=0, & (x,y)\in D,\\ W(t,x,y,0)=0, & (x,y)\in D,\\ \boldsymbol{n}\cdot(\rho c\boldsymbol{v}W+k_1\nabla W)\Big|_{(x,y)\in\partial D}=0, & (x,y)\in\partial D,\\ W(t_{i+1},x,y,z)=0, & (x,y,z)\in\Omega.\end{cases} \tag{3.4}$$

We have

$$\begin{aligned}&\int_{t_i}^{t_{i+1}}\int_{\Omega}\left\{W\left[\rho c\left(\frac{\partial(\delta T)}{\partial t}+\boldsymbol{v}\cdot\nabla(\delta T)\right)-\nabla\cdot(k_1\nabla(\delta T))\right]\right\}\\ &\quad+\left\{\delta T\left[\rho c\left(\frac{\partial W}{\partial t}+\nabla\cdot(\boldsymbol{v}W)\right)+\nabla\cdot(k_1\nabla W)\right]\right\}\\ &=-\int_{t_i}^{t_{i+1}}\int_{\Omega}\left[W\delta\boldsymbol{v}\cdot\nabla T+\sum_{j=1}^{m}\delta T\zeta_j(t)\delta(\boldsymbol{x}-\boldsymbol{x}_j)\right].\end{aligned}$$

Since

$$\int_{t_i}^{t_{i+1}}\int_{\Omega}W\rho c\frac{\partial(\delta T)}{\partial t}+\delta T\rho c\frac{\partial W}{\partial t}=\int_{\Omega}\rho c(W\delta T)|_{t_i}^{t_{i+1}}=0,$$

$$\begin{aligned}&\int_{t_i}^{t_{i+1}}\int_{\Omega}(W\rho c\boldsymbol{v}\cdot\nabla(\delta T)+\delta T\rho c\nabla\cdot(\boldsymbol{v}W))\\ &\quad=\int_{t_i}^{t_{i+1}}\rho c\int_{\partial\Omega}W\delta T\boldsymbol{v}\cdot\boldsymbol{n}=\int_{t_i}^{t_{i+1}}\delta T(\boldsymbol{n}\cdot\rho c\boldsymbol{v}W)|_{(x,y)\in\partial D},\end{aligned}$$

$$\begin{aligned}&\int_{t_i}^{t_{i+1}}\int_{\Omega}(-W\nabla\cdot(k_1\nabla(\delta T))+\delta T\nabla\cdot(k_1\nabla W))\\ &\quad=\int_{t_i}^{t_{i+1}}\int_{\partial\Omega}(-Wk_1\nabla(\delta T)\cdot\boldsymbol{n}+\delta Tk_1\nabla W\cdot\boldsymbol{n})=\int_{t_i}^{t_{i+1}}\delta T(\boldsymbol{n}\cdot k_1\nabla W)|_{(x,y)\in\partial D},\end{aligned}$$

it follows that

$$-\int_{t_i}^{t_{i+1}}\int_\Omega \delta \boldsymbol{v}\cdot\nabla TW=\int_{t_i}^{t_{i+1}}\int_\Omega\sum_{j=1}^m \delta T(t,\boldsymbol{x})\zeta_j(t)\delta(\boldsymbol{x}-\boldsymbol{x}_j)=\int_{t_i}^{t_{i+1}}\sum_{j=1}^m \delta T(t,\boldsymbol{x}_j)\zeta_j(t). \tag{3.5}$$

By comparing (3.5) with (3.3), we have

$$J_1'(\boldsymbol{v})=-\nabla TW.$$

A simple calculation yields the Fréchet derivative of the functional $J_2(\boldsymbol{v})$: $J_2'(\boldsymbol{v})=\alpha\boldsymbol{v}$. Therefore, to obtain the gradient, we need to solve the adjoint problem (3.4), which is a backward heat equation.

3.2 Update $S_0(x,y)$ when v is given

We update $S_0(x,y)$ from the current surface $S_N(x,y)=S(t_c,x,y)$ while assuming that velocity $\boldsymbol{v}$ is given. Let $\tilde{S}_0(x,y)=S_0(x,y)+\delta S_0(x,y)$, where S is the solution of the surface process model with the initial value $S_0(x,y)$ and $\tilde{S}$ is the solution with the initial value $\tilde{S}_0$. Let $\delta S=\tilde{S}-S$. Then δS satisfies the following equations

$$\begin{cases}\dfrac{\partial(\delta S)}{\partial t}=\nabla\cdot(k_2\nabla(\delta S))+\boldsymbol{u}\cdot\nabla(\delta S)+a\sqrt{Q}\boldsymbol{d}\cdot\nabla(\delta S),\\ \dfrac{\partial(\delta S)}{\partial n}\Big|_{\partial D}=0,\\ \delta S(t_0,x,y)=\delta S_0(x,y),\qquad (x,y)\in D,\quad t_p\le t\le t_c.\end{cases} \tag{3.6}$$

Suppose that $S_c(x,y)$ is the measured surface at current time t_c and $S(t_N,x,y)$ is the numerically reconstructed surface with the initial value $S_0(x,y)$.

Define the cost functional

$$I(S_0)=\frac{1}{2}\int_D(S(t_N,x,y)-S_c(x,y))^2+\beta\int_D|S_0|^2=I_1+I_2. \tag{3.7}$$

We apply the gradient method to minimize the cost functional defined in (3.7). Thus

$$I_1(\tilde{S}_0)-I_1(S_0)=\frac{1}{2}\int_D\delta S(t_N,x,y)(\tilde{S}(t_N,x,y)+S(t_N,x,y)-2S_c(x,y)). \tag{3.8}$$

Therefore

$$I_1'(S_0)\delta S_0=\int_D S'(t_N,x,y)\delta S_0(S(t_N,x,y)-S_c(x,y)),$$

where S' is the Fréchet derivative with respect to the initial surface. To evaluate the gradient $I_1'(S_0)$ of the functional $I(S_0)$, we introduce the adjoint problem

$$\begin{cases}\dfrac{\partial V}{\partial t}=-\nabla\cdot(k_2\nabla V)+\nabla\cdot(\boldsymbol{u}V)+\nabla\cdot(a\sqrt{Q}\boldsymbol{d}V),\\ \dfrac{\partial V}{\partial n}\Big|_{\partial D}=0,\\ V(t_c,x,y)=S(t_c,x,y)-S_c(x,y),\qquad (x,y)\in D.\end{cases} \tag{3.9}$$

Combining (3.6) with (3.9), we have

$$\int_{t_p}^{t_c}\int_D V\left[\frac{\partial(\delta S)}{\partial t}-\nabla\cdot(k_2\nabla(\delta S))-\boldsymbol{u}\cdot\nabla(\delta S)-a\sqrt{Q}\boldsymbol{d}\cdot\nabla(\delta S)\right]$$
$$+\delta S\left[\frac{\partial V}{\partial t}+\nabla\cdot(k_2\nabla V)-\nabla\cdot(\boldsymbol{u}V)-\nabla\cdot(a\sqrt{Q}\boldsymbol{d}V)\right]=0.$$

Since

$$\int_{t_p}^{t_c}\int_D \delta S\frac{\partial V}{\partial t}+V\frac{\partial(\delta S)}{\partial t}=\int_D (V\delta S)|_{t_p}^{t_c}=\int_D((S(t_c)-S_c)\delta S(t_c)-V(t_p)\delta S_0),$$
$$\int_{t_p}^{t_c}\int_D \delta S\nabla\cdot(k_2\nabla V)-V\nabla\cdot(k_2\nabla(\delta S))=\int_{t_p}^{t_c}\int_{\partial D}\delta S k_2\frac{\partial V}{\partial n}-Vk_2\frac{\partial(\delta S)}{\partial n}=0,$$
$$\int_{t_p}^{t_c}\int_D \delta S\nabla\cdot(\boldsymbol{u}V)+V\boldsymbol{u}\cdot\nabla(\delta S)=\int_{t_p}^{t_c}\int_{\partial D}\delta SV\boldsymbol{u}\cdot\boldsymbol{n}=0,$$
$$\int_{t_p}^{t_c}\int_D \delta S\nabla\cdot(a\sqrt{Q}\boldsymbol{d}V)+Va\sqrt{Q}\boldsymbol{d}\cdot\nabla(\delta S)=\int_{t_p}^{t_c}\int_{\partial D}\delta Sa\sqrt{Q}\boldsymbol{d}\cdot\boldsymbol{n}=0,$$

we obtain

$$\int_D (S(t_c)-S_c)\delta S(t_c)=\int_D V(t_p)\delta S_0. \tag{3.10}$$

By comparing (3.10) with (3.8), we derive the gradient of the cost functional as $I_1'(S_0)=V(t_p,x,y)$. Similarly, we may easily get the Fréchet derivative of the functional I_2: $I_2'(S_0)=\beta S_0$. Therefore, the gradient of the cost functional (3.7) can be evaluated through solving the adjoint problem (3.9).

3.3 A modification of the inverse problem for HTPM

It is evident that additional information on the data to be recovered certainly enhances the accuracy of the numerical reconstruction. For example, a priori knowledge (through sampling) of the direction or distribution of the velocity field can lead to the simplification

$$\boldsymbol{v}=v\cdot\boldsymbol{d},$$

where v is unknown but $\boldsymbol{d}$ is known. The governing equation (2.2) is replaced by a slightly modified version

$$\begin{cases}
\rho c\left(\dfrac{\partial T}{\partial t}+v\boldsymbol{d}\cdot\nabla T\right)=\nabla\cdot(k\nabla T)+\rho H, & (x,y,z)\in\Omega,\ 0\le t\le t^*,\\
T(t,x,y,S(t,x,y))=T_a, & (x,y)\in D,\ 0\le t\le t^*,\\
T(t,x,y,0)=T_c, & (x,y)\in D,\ 0\le t\le t^*,\\
\dfrac{\partial T}{\partial n}\Big|_{(x,y)\in\partial D}=0, & (x,y)\in\partial D,\ 0\le t\le t^*,\\
T(0,x,y,z)=T_0(x,y,z), & (x,y,z)\in\Omega,\ 0\le t\le t^*.
\end{cases} \tag{3.11}$$

For the inverse problem, the observation data is one measurement of the temperature T at time t^*, which is denoted as $Z(x,y,z)$. Similarly, we define the cost functional

$$J(\boldsymbol{v})=\frac{1}{2}\int_\Omega (T(t^*;\boldsymbol{x})-Z)^2+\alpha\int_\Omega |\boldsymbol{v}|^2=J_1+J_2.$$

Let $\zeta=T(t^*;\boldsymbol{x})-Z$. Then

$$J_1(\tilde{\boldsymbol{v}})-J_1(\boldsymbol{v})=\frac{1}{2}\int_\Omega \delta T(t^*)(\tilde{T}(t^*)+T(t^*)-2Z).$$

Hence

$$J_1'(\boldsymbol{v})\delta\boldsymbol{v}=\int_\Omega T'(t^*)\delta\boldsymbol{v}\zeta$$

or

$$J_1'(\boldsymbol{v})=T'(t^*)\zeta.$$

Consider the adjoint problem

$$\begin{cases} \rho c\left(\dfrac{\partial W}{\partial t}+\nabla\cdot(\boldsymbol{v}W)\right)=-\nabla\cdot(k\nabla W), & \\ W(t,x,y,S(t,x,y))=0, & (x,y)\in D, \\ W(t,x,y,0)=0, & (x,y)\in D, \\ \boldsymbol{n}\cdot(\rho c\boldsymbol{v}W+k\nabla W)\Big|_{(x,y)\in\partial D}=0, & (x,y)\in\partial D, \\ W(t^*,x,y,z)=\zeta, & (x,y,z)\in\Omega. \end{cases} \tag{3.12}$$

We have

$$\begin{aligned} &\int_0^{t^*}\int_\Omega\left\{W\left[\rho c\left(\frac{\partial(\delta T)}{\partial t}+\boldsymbol{v}\cdot\nabla(\delta T)\right)-\nabla\cdot(k\nabla(\delta T))\right]\right\} \\ &\quad+\left\{\delta T\left[\rho c\left(\frac{\partial W}{\partial t}+\nabla\cdot(\boldsymbol{v}W)\right)+\nabla\cdot(k\nabla W)\right]\right\} \\ &=-\int_0^{t^*}\int_\Omega (W\delta\boldsymbol{v}\cdot\nabla T). \end{aligned}$$

Since

$$\int_0^{t^*}\int_\Omega\left(W\rho c\frac{\partial(\delta T)}{\partial t}+\delta T\rho c\frac{\partial W}{\partial t}\right)=\int_\Omega \rho c(W\delta T)|_0^{t^*}=\int_\Omega \rho c\zeta\delta T(t^*),$$

$$\begin{aligned} &\int_0^{t^*}\int_\Omega (W\rho c\boldsymbol{v}\cdot\nabla(\delta T)+\delta T\rho c\nabla\cdot(\boldsymbol{v}W) \\ &\quad=\int_0^{t^*}\rho c\int_{\partial\Omega}W\delta T\boldsymbol{v}\cdot\boldsymbol{n}=\int_0^{t^*}\delta T(\boldsymbol{n}\cdot\rho c\boldsymbol{v}W)|_{(x,y)\in\partial D}, \end{aligned}$$

and

$$\begin{aligned}&\int_0^{t^*}\int_\Omega -W\nabla\cdot(k\nabla(\delta T))+\delta T\nabla\cdot(k\nabla W)\\ =&\int_0^{t^*}\int_{\partial\Omega}(-Wk\nabla(\delta T)\cdot\boldsymbol{n}+\delta Tk\nabla W\cdot\boldsymbol{n})=\int_0^{t^*}\delta T(\boldsymbol{n}\cdot k\nabla W)|_{(x,y)\in\partial D},\end{aligned}$$

we obtain

$$-\int_0^{t^*}\int_\Omega \delta\boldsymbol{v}\cdot\nabla TW=\int_\Omega \rho c\delta T(t^*)\zeta.$$

Thus

$$J_1'(\boldsymbol{v})\delta\boldsymbol{v}=-\frac{1}{\rho c}\int_0^{t^*}\int_\Omega \delta\boldsymbol{v}\cdot\nabla TW$$

or

$$J_1'(v)=-\frac{1}{\rho c}\boldsymbol{d}\cdot\nabla TW.$$

4 Numerical results

In this section, we present several numerical test results to validate our model. The following experimental data for parameters are used in the governing equation for our numerical computation purpose:

- Heat transport diffusivity: 32 km^2/myr.
- velocity: on the scale of 1.0 km/myr.
- ρ: 2700 kg/m^3.
- c: heat capacity 800 J/(kg K).
- H: radiogenic production 0.5 $\mu W/\text{m}^3$.
- $T_a=293K$, $T_m=1073K$.

For the numerical computation, we use the following setup:

- The computational domain: $x\in[0,100]$ km, $y\in[0,50]$ km, $z\in[0,S(x,y)]$ km; each time interval is separated into 20 time steps.
- The regularization parameter: $\alpha=10^{-3}$, $\beta=10^{-6}$.
- Measurement data: $T(t_c,\mathbf{x}_j(t_c))$, temperature on nodes in Subsection 4.1.
- Measurement data: $S(t_c,x_j,y_j)$, lift of surface on nodes in Subsection 4.2.
- Measurement data: $\{T(n\triangle t,\mathbf{x}_j(n\triangle t))\}|_{n=1}^N$ and $S(t_c,x_j,y_j)$ on nodes in Subsection 4.3.

To create the mesh for the finite element method, we employ a simple and effective mesh generator in MATLAB by Persson and Strang [18] for 3D HTPM. In the spatial domain Ω, we choose the continuous piecewise linear polynomial. In the temporal domain, we use the backward Euler method. All of the numerical experiments are performed in a Window XP machine with an Inter(R) Pentium(R) 4, 3.20GHz, 3.19 GHz CPU and 2.00GB of RAM.

4.1 Backward for HTPM

We run the numerical simulation on one time interval $t_c - \triangle t \leq t \leq t_c$, $t_c = 5\times 10^5$, $\triangle t = 1\times 10^5$.

Test 1 We begin with the simplest case in which the velocity field is composed of a two-component piecewise constant. The direction is also assumed to be known. The data to be restored is the magnitude. We use the heat transport model within the fixed domain to solve a coefficient inverse problem for reconstructing the simple velocity field. For simplicity, we assume zero velocity in the x direction, though our algorithm and computation may be extended to the three dimensional case. We use one measurement of the temperature at the end of time period for the observation. Fig. 1 is the profile of the velocity field. Table 1 shows the reconstruction accuracy.

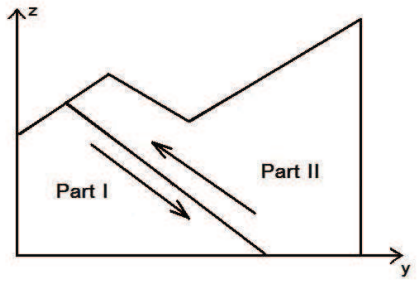

Figure 1: Two component piecewise constant velocity field.

Test 2 The velocity field is assumed to be composed of four piecewise constants. Once again, the direction is known and the magnitude is what we need to reconstruct. Fig. 2 and Table 2 show the velocity profile and accuracy of restoration, respectively.

Test 3 As expected, the numerically recovered velocity field is consistent with the exact data for the last two setup. For now, we test our numerical method for a velocity field which is composed of four parts. For each part, the direction is an unknown. The result in Table 3 shows that the reconstruction is less accurate due to the more information to be restored. And it gets better when we drop the unresolved boundary layer or when we refine the mesh, which means more information is at our disposal and high numerical accuracy.

Table 1: Numerical result: Two component piecewise constant velocity field.

relative error	iterations	elements
$77\% \to 0.3\%$	27	17070

Table 2: Numerical result: Four component piecewise constant velocity field.

relative error	iterations	elements
$84\% \to 0.5\%$	42	17070

Table 3: Numerical result: Four component piecewise variable velocity field.

relative error	drop boundary	drop two layers	iterations	elements
$87\% \to 37\%$	$87\% \to 16\%$	$87\% \to 8\%$	583	17070
$87\% \to 24\%$	$87\% \to 7\%$	$87\% \to 3\%$	807	31687

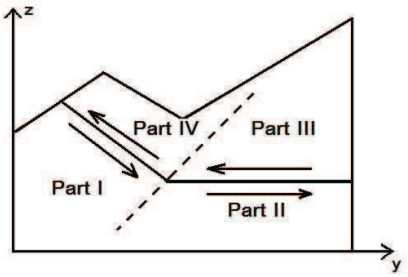

Figure 2: Four component piecewise constant velocity field.

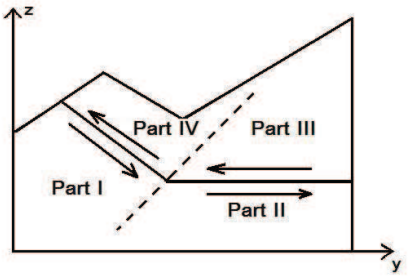

Figure 3: Four component piecewise variable velocity field.

4.2 Model IV (Backward for SPM)

We run the numerical simulation on one time interval $t_c - \triangle t \le t \le t_c$, $t_c = 5\times 10^5$, $\triangle t = 1\times 10^5$. The algorithm for the surface process model is much simpler than for the heat transportation process model because the surface process model is a linear problem. Nevertheless, it is also a typical backward parabolic problem. The reconstruction of the initial value is extremely ill-posed. Although to reconstruct the initial value is not stable, the reconstruction at any time t, $t_p < t < t_c$, is better. The reconstruction is better if time t is closer to t_c. In this subsection, we present a numerical result at initial time and at half time. The initial surface is

$$S_p(x,y) = (\cos(\pi \times x/100) + \cos(\pi \times y/50)) \times 2 + 20.$$

Fig. 4 shows the exact and reconstructed initial surface. Fig. 5 shows the exact and numerically restored surface at the middle of this time period. Table 4 shows the accuracy of restoring surface to the past.

Table 4: Accuracy of the reconstruction.

initial guess	relative error	computational cost
$S(x,y)=15$	$23\%\rightarrow 0.3\%$	13 seconds

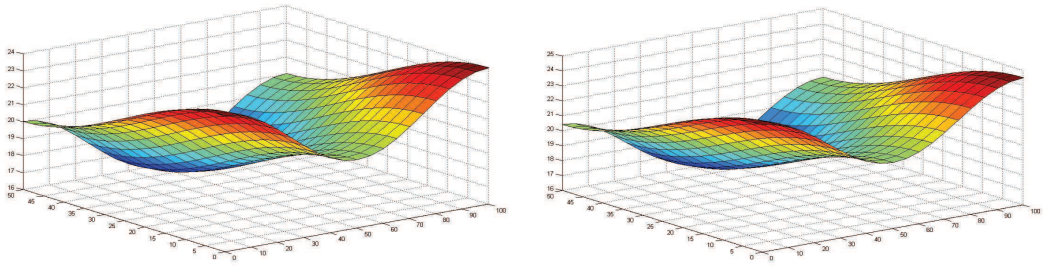

Figure 4: Left: Exact initial surface; Right: Reconstructed initial surface.

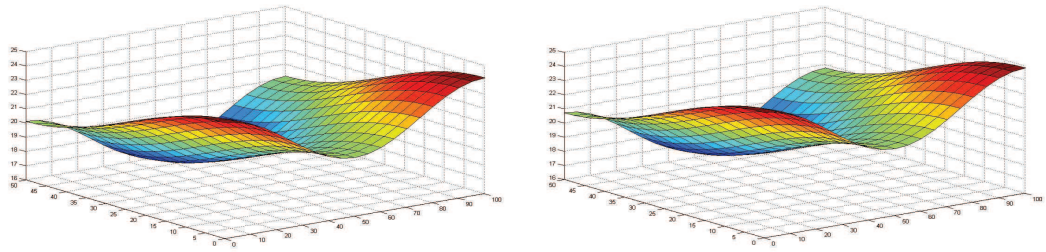

Figure 5: Left: Exact half-time surface; Right: Reconstructed half-time surface.

4.3 Model V: The coupled system

We run the numerical simulation on one time interval $t_p=0\leq t\leq t_c$, $t_c=5\times 10^5$, $\triangle t=1\times 10^5$. For the coupled system, the main challenge is the slow convergence of the iterations, thus there is a large computational cost. We test our method on the case that velocity field is composed of four parts, for each part the direction of the velocity is known. In order to test stability of the algorithm, we also add 5% random noise to the measurement data. We compare the two figures in Fig. 7, the exact initial surface and the numerically reconstructed surface. It shows that the main feature of the surface is restored correctly and the accuracy shown in the Table 6 is satisfactory. Fig. 6 is the velocity profile.

We choose the velocity in the Table 5 as the exact velocity field, in which each row is corresponding to the velocity for one time interval.

5 Conclusion

Successful reconstruction of the mountain surface often provides geologists with a valuable perspective about the limit of the range that thermochronometer data can be interpreted. In this paper, we have presented a novel inverse problem method along with

Table 5: Velocity field.

Time interval	v_y				v_z			
N	I	II	III	IV	I	II	III	IV
1	1	1.5	-2	-1.3	-1	0	0	1.3
2	0.8	1.5	-2	-1.4	-0.8	0	0	1.4
3	0.8	1.2	-1.7	-1.3	-0.8	0	0	-.3
4	1	1.5	-1.8	-1.5	-1	0	0	1.5
5	1.2	1.5	-2	-1.5	-1.2	0	0	1.5

Table 6: Reconstruction without random noise to the measurement data.

initial guess	relative error	computational cost	elements
$S(x,y)=15$	$23\%\rightarrow 2\%$	18 hours	17070

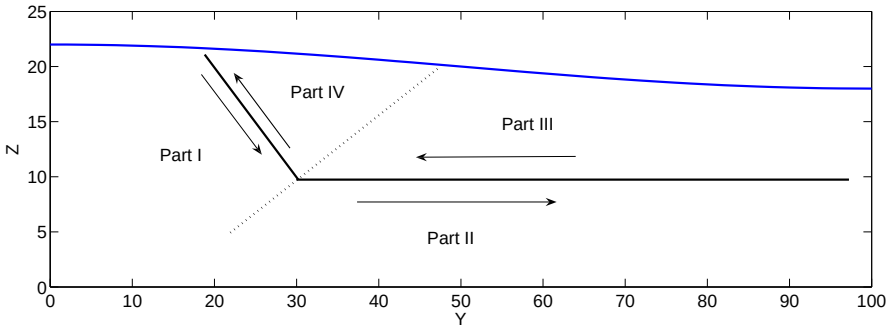

Figure 6: Four component piecewise constant velocity field.

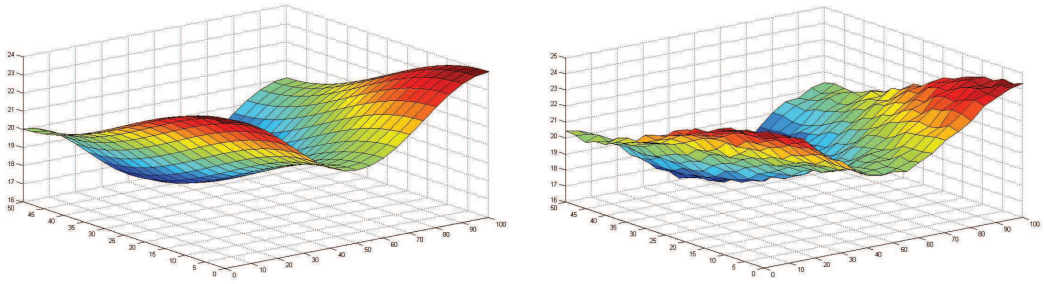

Figure 7: Left: Exact initial surface; Right: Reconstructed initial surface.

the new algorithms and numerical examples. Our method provides a solid and essential mean in understanding how to reconstruct the evolution of mountain topography efficiently and accurately. We have also presented the mathematical model formulation by taking account of the main factors affecting temperature distribution in the mountain, such as heat transferring in the mountain, heat produced by the radiological element in rocks whose history temperature can be used for observation. As the initial step, we

have tested our models on very simple cases to obtain promising numerical results. Even with a limited amount of data, our results have demonstrated the restored surface carries important features of the (exact) initial surfaces for the test problems. Our general computational approach may be extended to a range of other tectonic and geomorphic settings where the kinematic and topographic history could be different.

Our long term objective is to develop a systematic tool for the understanding of dynamic geological processes influenced by thermal factors. A significant inherent challenge is to produce accurate numerical approximation of the large scale problem over million year time scales.

We conclude the paper by some general remarks about future directions along this line of research. There are many other factors affecting the temperature distribution that are neglected in our governing equations. An interesting future direction is to include also the melting effect which would lead to a highly nonlinear equation. The corresponding inverse problem for the nonlinear forward problem is at present completely open. Another interesting open problem is to numerically solve the problem with more realistic setups so that the measurement data is $T(t,\boldsymbol{x}_j(t))$, $j=1,\cdots,m$, the history temperature data at rocks $\boldsymbol{x}_j(t)$ carrying radiogenic elements. Mathematically, an interesting problem is to study the uniqueness question for the coefficient inverse problem given the direction of the velocity field. There are also many challenging issues for developing fast and efficient algorithms for solving the large scale model problem.

Acknowledgments

The research of G. Bao, Y. Wang, and Z. Xu was supported in part by the NSF CMG grant EAR-0724527, and NSF grant EAR-0724656 to T. Ehlers and P. Li.

References

[1] Alik, I.Z., Gerald, S., Igor, T. and Alexander, K., Inverse problem of thermal convection: numerical approach and application to mantle plume restoration, Physics of the Earth and Planetary Interiors. 145(2004), 99-114.

[2] Baldwin, S.L., Monteleone, B.D., Webb, L.E., Fitzgerald, P.G., Grove, M. and Hill, E.J., Pliocene eclogite exhumation at plate tectnoic rates ineastern Papua New Gunea, Nature. 431(2004), 263-267.

[3] Braun, J. and Sambridge, M., A new method based on irregular spatial discretization, Basin Research. 9(1997), 27-52.

[4] Bukhgeim, A.L., Introduction to the Theory of Inverse Problems, The Netherland: VSP. 2000.

[5] Colton, D., The approximation of solutions to the backwards heat equation in a nonhomogeneous medium, J. Math. Anal. Appl. 72(1979), 418-429.

[6] Choulli, M. and Yamamoto, M., Some stability estimates in determing sources and coefficients, J. Inv. Ill-posed Problems. 14(2006), 355-373.

[7] Dodson, M.H., Closure temperature in cooling geochronological and petreological systems, Contrib. Minerol. Petrol. 40(1973), 259-274.

[8] Ehlers, T.A., Farley, K.A., Apatite(U-Th)/He thermochronometry: methods and applications to problems in tecnoics and surface processes, EPSL-Frontiers. 206(2003), 1-14.
[9] Ehlers, T.A., Farley, K.A., Rusmore, M.E. and Woodsworth, G.J., Apatite(U-Th)/He signal of large magnitude and accelerated glacial erosion: Southwest Britishi Columbia, Geology. 34(2006), 765-768.
[10] Elden, L., Time discretization in the backward solution of parabolic equations, Math. Comput. 39(1982), 53-84.
[11] Gallagher, K., Evolving thermal histories from fission track data, Earth Planet Sci Lett. 136(1995), 421-435.
[12] Haenel, R., Rybach, L. and Stegena, L., Handbook of Terrestrial Heat-Flow Density Determination, Kluwer Academic Publishers, 1988.
[13] Herman, F., Braun, J., Senden, T.J. and Dunlap, W.J., (U-Th)/He thermochronometry: Mapping 3D geometry using micro-x-ray tomography and solving the associated production-diffusion equation, Chemical Geology. 242(2007), 126-136.
[14] Ismail-Zadeh, A.T., Talbot, C.J. and Volozh, Y.A.,Dynamic restoration of profiles across diapiric salt structures: numerical approach and its applications, Tectonophysics. 337(2001a), 21-36.
[15] Isakov, V, Inverse Problems for Partial Differential Equations, Springer, New York, 1998.
[16] Ivanov, V.K., Vasin, V.V. and Tanana, V.P.,Theory of Linear Ill-Posed Problems and Its Applications [in Russian], Nauka, Moscow, 1978.
[17] Lutz, T.M. and Omar, G., An inverse method of modeling thermal histories from apatite fission track data, Earth Planet. Sci. Lett. 104(1991), 181-195.
[18] Persson, P. and Strang, G., A simple mesh generator in Matlab, SIAM Rev. 46(2004), 329-345.
[19] Tikhonov, A.N. and Arsenin, V.A., Solution of Ill-posed Problems, Winston, Washington, DC, pp255. 1977.
[20] Shuster, D.L. and Farley, K.A., 4He/3He themochronometry: theory, practice, and potential applications, Rev. in Mineralogy and Geochemistry. 58,(2005), 181-203.
[21] Whipp, D.M. and Ehlers, T.A., Influence of goundwater flow on thermochronometer derived exhumation rates in the Nepalese Himalaya, Geology. 35(2007), 851-854.
[22] Wolf, R.A., Farley, K.A. and Silver, L.T., Assessment of (U-Th)/He thermochronometry: the low tempratrue history of the San Jacinto Mountains, California. Geology. 25(1997), 65-68.
[23] Yamamoto, M. and Zou, J., Simultaneous reconstrction of the intial temtperature and heat radiative coefficient, Inverse Problems. 17(2001), 1181-1202.